

Received 5 March 2018; revised 9 April 2018; accepted 8 May 2018. Date of publication 15 May 2018;  
date of current version 8 June 2018. The review of this paper was arranged by Editor C. Surya.

Digital Object Identifier 10.1109/JEDS.2018.2835160

# Influence of Surface Energy and Roughness on Hole Mobility in Solution-Processed Hybrid Organic Thin Film Transistors

SUNGSIK LEE<sup>ID 1,2</sup> (Member IEEE), FLORA M. LI<sup>2,3</sup>, AND AROKIA NATHAN<sup>ID 2</sup> (Fellow IEEE)

<sup>1</sup> Department of Electronics Engineering, Pusan National University, Pusan 46241, South Korea

<sup>2</sup> Department of Engineering, University of Cambridge, Cambridge CB3 0FA, U.K.

<sup>3</sup> Department of Information Technology, Apple Inc., Cupertino, CA 95014, USA

CORRESPONDING AUTHORS: S. LEE AND A. NATHAN (e-mail: sungsiklee@pusan.ac.kr; an299@cam.ac.uk)

This work was supported by Pusan National University Research Grant, 2017, and Basic Science Research Program through the National Research Foundation of Korea funded by the Ministry of Science, ICT and Future Planning under Grant 2018R1C1B6001688, in part by the EU projects DOMINO under Grant 645760, and in part by BET-EU under Grant 692373.

**ABSTRACT** We investigate the influence of the surface energy and roughness on the hole mobility in organic thin-film transistors where a poly(3,3'''-dialkylquarterthiophene) (PQT-12) hybridized with an octyltrichlorosilane self-assembled monolayer is employed as the semiconducting layer on a silicon nitride ( $\text{SiN}_x$ ) gate insulator. Here, these surface properties are modified with varying the duration of oxygen plasma treatments on the  $\text{SiN}_x$  surface, eluding to a different surface roughness and energy. From our analysis coupled with the experimental results, it is found that the surface roughness ( $R_a$ ) controls the degree of surface roughness scattering ( $\chi_{\text{SR}}$ ) while the surface energy ( $E_S$ ) determines the reference mobility ( $\mu_b$ ), yielding the effective hole mobility expressed as a product of two terms associated with  $\mu_b$  and  $\chi_{\text{SR}}$ , respectively. It is found that  $\mu_b$  follows a power law as a function of  $E_S$ , and  $\chi_{\text{SR}}$  grows exponentially with increasing  $R_a$ . In addition, a characteristics scattering length ( $\lambda_c$ ) appears in the mobility expression, which turns out to be a demarcation, suggesting that  $R_a$  is required to be at least smaller than  $\lambda_c$  to minimize  $\chi_{\text{SR}}$ .

**INDEX TERMS** Organic thin film transistors, surface roughness scattering, surface energy, hole mobility.

## I. INTRODUCTION

Organic semiconductors are one of the promising candidates for large area applications since they can meet a mechanical flexibility and low-temperature processability [1]–[5]. The latter mainly stems from the ability of a solution-based processing and ink-jet printing [6], [7]. In an organic device fabricated in such processes, an electrical performance, e.g., hole mobility, largely relies on the quality of the dielectric-semiconductor interface besides the degree of structural disorder in the semiconductor layer [8], [9]. Here, the quality of the dielectric-semiconductor interface and the molecular ordering of the organic semiconductor layer have a strong bearing on the field-effect hole mobility. Those issues are also severe in inorganic materials formed with a solution-based fabrication process. Here, the role of surface properties is crucial to determine an inorganic material-based transistor

performance [10], [11]. As an example of organic materials, a poly(3,3'''-dialkylquarterthiophene) (PQT-12) TFT with a silicon nitride ( $\text{SiN}_x$ ) gate insulator can have different interfacial properties and respective hole mobilities, depending on a dielectric surface treatment by either inserting a self-assembled monolayer (SAM) or applying an oxygen ( $\text{O}_2$ ) plasma treatment on the  $\text{SiN}_x$  surface [12], [13]. Here, a quantitative investigation is required to physically explain the influences of these surface properties affect the hole mobility.

In this letter, we present a quantitative analysis on how surface roughness ( $R_a$ ) and surface energy ( $E_S$ ) physically affect the hole mobility in solution-processed organic TFTs. In the examined device, we employed a PQT-12 organic semiconductor layer hybridized with the octyltrichlorosilane (OTS) SAM on the  $\text{SiN}_x$  gate insulator. Here, as the key factor to

vary the interfacial properties, the O<sub>2</sub> plasma treatment is performed on the SiN<sub>x</sub> gate insulator surface, whose duration is experimentally varied to modify the SiN<sub>x</sub> surface yielding different R<sub>a</sub> and E<sub>S</sub>. In our analysis coupled with the results from these experiments, we assume the distribution of the surface roughness follows a Gaussian probability function with the mean value of R<sub>a</sub> while introducing a characteristics scattering length ( $\lambda_c$ ). Besides, we use the Owens-Wendt method to retrieve E<sub>S</sub> from the contact angle of water on the OTS SAM surface. Based on this, the modelled results indicate that R<sub>a</sub> determines the degree of the surface roughness scattering ( $\chi_{SR}$ ) which grows exponentially with increasing R<sub>a</sub>, and the reference mobility ( $\mu_b$ ) is governed by E<sub>S</sub> following a power-law. These yield the hole mobility relation as  $\mu_b(1 - \chi_{SR})$ . In addition, it is suggested that  $\lambda_c$  can be treated as a demarcation to determine how much R<sub>a</sub> needs to be reduced to minimize the surface roughness scattering.

## II. RESULTS AND DISCUSSION

### A. DEVICE PREPARATIONS

The examined TFTs were fabricated on a highly-doped silicon substrate which serves as the gate along with thermally-evaporated Cr-Au source/drain contacts and spin-coated PQT-12 as the semiconductor layer, as shown in Fig. 1(a). In particular, SiN<sub>x</sub> as the gate dielectric was formed by plasma enhanced chemical vapour deposition (PECVD) at 150°C for a plastic substrate compatibility. After the deposition of SiN<sub>x</sub>, the O<sub>2</sub> plasma treatment was carried out using a reactive ion etching (RIE) system with a chamber pressure of 150 mTorr and RIE power of 34 W. After that, the OTS SAM was formed by immersing the substrates in a 0.1M solution of OTS in toluene for 20 min at 60°C, followed by rinsing with toluene and isopropanol. These surface treatments were done prior to deposition of the PQT-12 layer. Electrical characterization of the OTFTs was carried out with a KEITHLEY 4200-SCS parameter analyzer. Surface properties were characterized using contact angle measurements for surface wettability and atomic force microscopy (AFM) measurements for surface roughness.

### B. DIFFERENT SURFACE TREATMENTS AND HOLE MOBILITY

Fig. 1(b) shows the drain current (I<sub>DS</sub>) vs. gate voltage (V<sub>GS</sub>) measured at -60V drain voltage (V<sub>DS</sub>) of PQT-12 OTFTs with 4 different types of surface treatments on SiN<sub>x</sub> gate dielectric. Note that the amplitude of drain and gate voltages can be reduced with usage of a larger gate-insulator capacitance which can scale-down the threshold voltage, thus a low voltage operation [14], [15]. With this saturation I-V data, field-effect mobility ( $\mu_{FE}$ ) is retrieved with the following relation,

$$\mu_{FE} = \frac{1}{0.5(W/L)C_{ox}} \left( \frac{d\sqrt{|I_{DS}|}}{dV_{GS}} \right)^2, \quad (1)$$

where W is the channel width, L channel length, and C<sub>ox</sub> gate-insulator capacitance. Also, an effective hole mobility ( $\mu_{eff}$ ) is captured as the peak value of  $\mu_{FE}$  for each

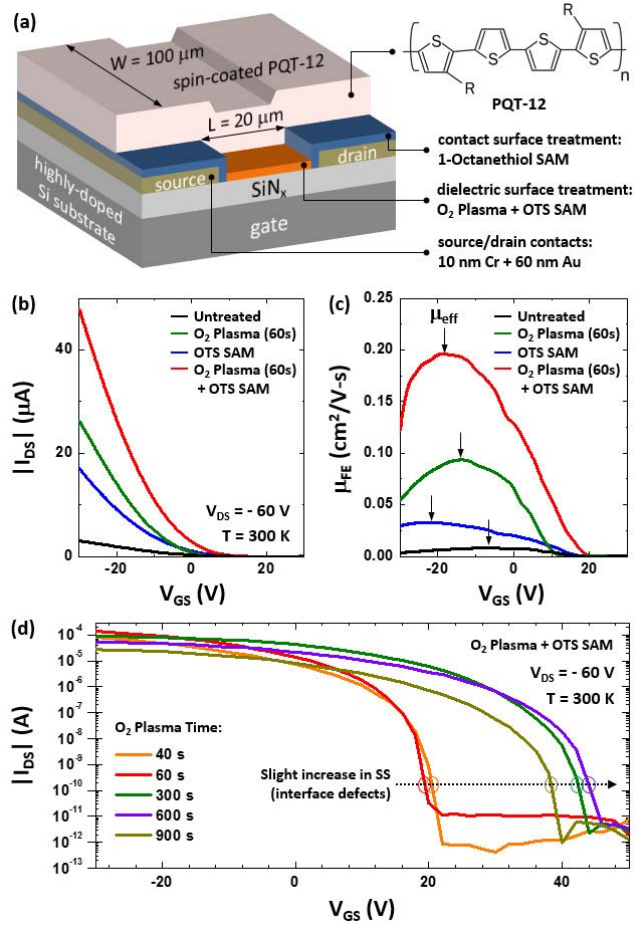


**FIGURE 1.** (a) Schematic cross-section of the hybrid PQT-12 OTFT structure considered in this study. (b) Saturation transfer characteristics (i.e., I<sub>DS</sub> vs. V<sub>GS</sub>) measured at V<sub>DS</sub> = -60V for different surface treatments. (c) Field-effect mobility ( $\mu_{FE}$ ) retrieved from the measured I-V. Here, the effective hole mobility ( $\mu_{eff}$ ) is captured as a peak value for each case. (d) I<sub>DS</sub> vs. V<sub>GS</sub> measured at V<sub>DS</sub> = -60V for the case of the O<sub>2</sub> plasma + OTS SAM while varying the oxygen plasma time.

case. As seen in Fig. 1(c),  $\mu_{eff}$  is increased with the 60s O<sub>2</sub> plasma treatment. Furthermore, the O<sub>2</sub> plasma treatment coupled with the OTS SAM (i.e., O<sub>2</sub> plasma + OTS SAM) provides the largest  $\mu_{eff}$ . This suggests that the combined treatment (O<sub>2</sub> plasma + OTS SAM) is one of the optimum ways to maximize the hole mobility further than the case for the O<sub>2</sub> plasma treatment only. For a further optimization of this case, the devices by the O<sub>2</sub> plasma + OTS SAM were further tested with varying the O<sub>2</sub> plasma time as seen in Fig. 1(d). Here, it is found that the sub-threshold slope (SS) is slightly increased with treatments for a longer plasma time > 60s, as retrieved in Fig. 2(a). This suggests that the interface quality is slightly degraded with a longer plasma time. For the above-threshold transfer characteristics, using Eq. (1), the  $\mu_{eff}$  is extracted as a function of O<sub>2</sub> plasma duration (see Fig. 2(b)). A peak in  $\mu_{eff}$  was observed at 60 s duration, which represents a 6.3-fold increase in mobility compared to devices without O<sub>2</sub> plasma exposure

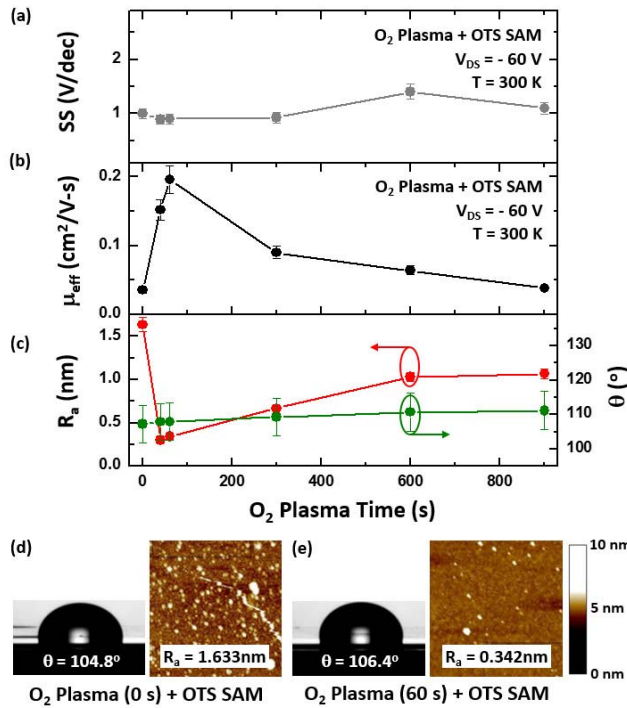


**FIGURE 2.** (a) Sub-threshold slope (SS) and (b) Effective hole mobility ( $\mu_{\text{eff}}$ ) as a function of the O<sub>2</sub> plasma time on SiN<sub>x</sub> surface prior to the OTS SAM formation. Here, 5% error-bars are shown. (c) Water contact angle ( $\theta$ ) and mean value of the surface roughness ( $R_a$ ) as a function of the O<sub>2</sub> plasma duration along with 5% error-bars. (d)  $\theta$  and AFM images for the O<sub>2</sub> plasma exposure time = 0 s and (e)  $\theta$  and AFM images for the O<sub>2</sub> plasma exposure time = 60 s, respectively.

(i.e., exposure time = 0 s). For longer exposures ( $t > 60$  s),  $\mu_{\text{eff}}$  gradually decreases. To understand these results in terms of surface properties, we examined the contact angle and surface roughness for the sample by the O<sub>2</sub> plasma + OTS SAM. Fig. 2(c) shows that the examined samples have a large contact angle ( $\theta > 100^\circ$ ) which is slightly changed with a different oxygen plasma time (see also Figs. 2(d) and (e)). This is mainly attributed to a hydrophobicity induced with the O<sub>2</sub> plasma treatment [16]–[18], and a hydrophobic surface of the OTS SAM [19]. As can be seen, a more distinctive correlation is observed between surface roughness ( $R_a$ ) and device mobility ( $\mu_{\text{eff}}$ ) in comparison with the contact angle. This implies that the surface energy is not so affected with the oxygen plasma. As illustrated in Figs. 2(b) and (c), there is a clear dependence of  $\mu_{\text{eff}}$  on  $R_a$ . Here, we observe an inverse behavior between  $\mu_{\text{eff}}$  and  $R_a$  as a function of the O<sub>2</sub> plasma time. At the plasma time  $\sim 60$  s, we have the maximum  $\mu_{\text{eff}}$  and almost minimum  $R_a$ . Here, it is suggested that the oxygen plasma duration of 40–60 s is an optimum. However, a longer plasma treatment gives rise to an over-etching while making  $R_a$  turn-around.

### C. SURFACE ENERGY AND REFERENCE MOBILITY

Evident from the above discussion is a dependence of mobility on contact angle and surface roughness. Here, we develop

a mathematical model to explain the relationships between these parameters. To account for contact angle effects in the mobility model, we first determine the surface energy ( $E_s$ ) value from the contact angle ( $\theta$ ) data. To calculate  $E_s$  from  $\theta$ , we used the Owens-Wendt method suitable for an OTS SAM surface [19], [20]

$$1 + \cos \theta = \frac{2}{E_L} \left[ \left( E_S^d E_L^d \right)^{0.5} + \left( E_S^h E_L^h \right)^{0.5} \right], \quad (2)$$

where  $E_L^d$  is the liquid's component of dispersion force,  $E_L^h$  the liquid's component of hydrogen bonding force,  $E_L (= E_L^d + E_L^h)$  the total surface tension/surface energy of the liquid,  $E_S^d$  the surface dispersion force component,  $E_S^h$  the hydrogen bonding force component of the surface, and  $E_S (= E_S^d + E_S^h)$  the surface energy. Assuming  $E_S^d \approx \alpha E_S^h$  and the ratio  $\alpha = 5$ ,  $E_S^d$  and  $E_S^h$  are calculated solving Eq. (2). Note that the ratio ( $\alpha$ ) between  $E_S^d$  and  $E_S^h$  on the same material is found to be constant for a narrow range of the contact angles [20], and  $\alpha = 5$  is empirically deduced for the OTS SAM surface. Using the contact angle data in Fig. 2(c),  $E_s$  is retrieved, as shown in Fig. 3(a). Here,  $E_L^d = 21.8$  mN/m,  $E_L^h = 51.0$  mN/m, and  $E_L = 72.8$  mN/m for water contact on the OTS SAM surface [19]. Based on  $E_s$ , the reference mobility ( $\mu_b$ ) at the surface is empirically represented as a power-law with the bulk band mobility ( $\mu_{\text{bulk}}$ ) of PQT-12,

$$\mu_b = \mu_{\text{bulk}} \left( \frac{E_s}{\zeta} \right)^{-\gamma}, \quad (3)$$

where  $\zeta$  is a reference surface energy and  $\gamma$  the power-law exponent. Here, the reference mobility ( $\mu_b$ ) may be associated with an interface defect density which is increased with a longer plasma time (see Fig. 2(a)). Using Eq. (3),  $\mu_b$  is drawn as a function of  $E_s$  for  $\zeta = 8.9$  mN/m and  $\gamma = 0.78$ . And  $\mu_{\text{bulk}}$  is to be 0.5 cm<sup>2</sup>/V-s. As shown in Fig. 3(b), it is found that  $\mu_b$  is decreased with increasing  $E_s$ .

### D. SURFACE ROUGHNESS SCATTERING AND EFFECTIVE MOBILITY

In addition, we describe the effective mobility ( $\mu_{\text{eff}}$ ) while considering surface roughness and energy,

$$\mu_{\text{eff}} = \mu_b \int_{-\infty}^{\infty} D_{SR}(x) \gamma_s(x) dx. \quad (4)$$

Here,  $\gamma_s(x)$  is the scattering factor along the channel depth (x), represented as  $\gamma_s(x) = \exp(-x/\lambda_c)$ ,  $\lambda_c$  is the characteristic scattering length, and  $D_{SR}(x)$  is the distribution of surface roughness along the channel depth (x). Note that  $\mu_b$  in Eq. (4) is employed as the pre-factor where the surface energy effect is considered through Eq. (3). For the distribution of the surface roughness, we employed a Gaussian random distribution represented as,

$$D_{SR}(x) = \frac{1}{\sqrt{2\pi}\sigma_{SR}} \exp \left[ -\frac{(x - R_a)^2}{2\sigma_{SR}^2} \right], \quad (5)$$

where  $R_a$  is the mean value of the surface roughness and  $\sigma_{SR}$  is the variance of the surface roughness. Solving Eq. (4) with

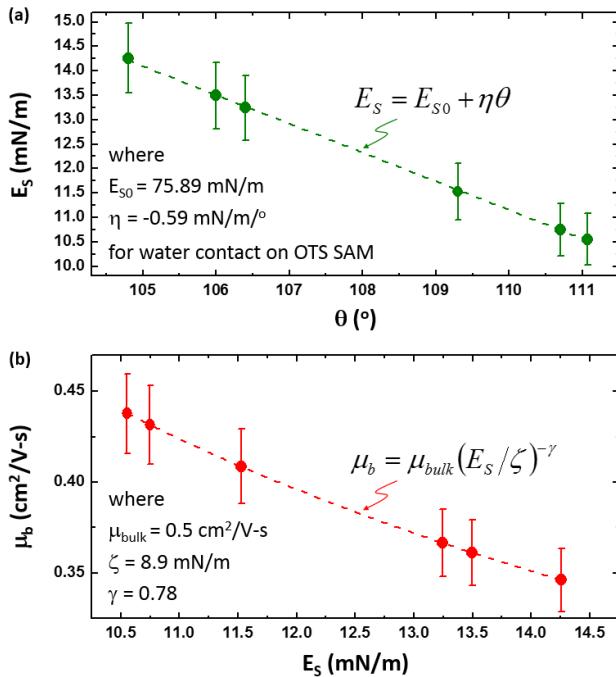


**FIGURE 3.** (a) Surface energy ( $E_S$ ) as a function of the water contact angle ( $\theta$ ), and (b) the reference mobility ( $\mu_b$ ) as a function of  $E_S$  on the OTS SAM surface, respectively. Here,  $E_{S0}$  is a constant as a intercept on the surface energy axis, and  $\eta$  is the slope with the contact angle. Here, 5% error-bars are shown.

Eq. (5), we can find an expression for the effective mobility ( $\mu_{\text{eff}}$ ) based on surface roughness ( $R_a$ ) as well as surface energy ( $E_S$ ),

$$\mu_{\text{eff}} = \mu_{\text{bulk}} \left( \frac{E_S}{\zeta} \right)^{-\gamma} \exp \left( -\frac{R_a}{\lambda_c} + \frac{\sigma_{SR}^2}{2\lambda_c^2} \right). \quad (6)$$

In order to capture the surface roughness effect, Eq. (6) can be rewritten as the ratio between  $\mu_{\text{eff}}$  and  $\mu_b$ ,

$$\frac{\mu_{\text{eff}}}{\mu_b} = \exp \left( -\frac{R_a}{\lambda_c} + \frac{\sigma_{SR}^2}{2\lambda_c^2} \right) \equiv 1 - \chi_{SR}, \quad (7)$$

where  $\chi_{SR}$  is defined as the degree of surface roughness scattering. Note that the value of  $\mu_{\text{eff}} / \mu_b$  is increased if less scattered with the surface roughness, thus  $\chi_{SR}$  is reduced. This implies an inverse proportionality between  $\mu_{\text{eff}} / \mu_b$  and  $\chi_{SR}$ . Since the maximum value of  $\mu_{\text{eff}} / \mu_b$  is unity, it should be expressed as  $1 - \chi_{SR}$  rather than  $1/\chi_{SR}$ . Using the values of  $\mu_{\text{eff}}$  and  $\mu_b$  seen in Fig. 4(a),  $1 - \chi_{SR}$  is plotted as a function of  $R_a$ , and a good agreement with the proposed model is achieved for  $\lambda_c = 0.517$  nm while assuming  $R_a \gg \sigma_{SR}$ , as shown in Fig. 4(b). Therefore, the mathematical model described here represents a practical means to quantitatively explain the dependence of mobility on both the surface energy and surface roughness.

Additionally, in the examined PQT-12 device treated with the O<sub>2</sub> plasma and OTS SAM,  $\lambda_c$  is found to be 0.517 nm, and  $\chi_{SR}$  is less than 0.5 when  $R_a < 0.517$  nm whereas it

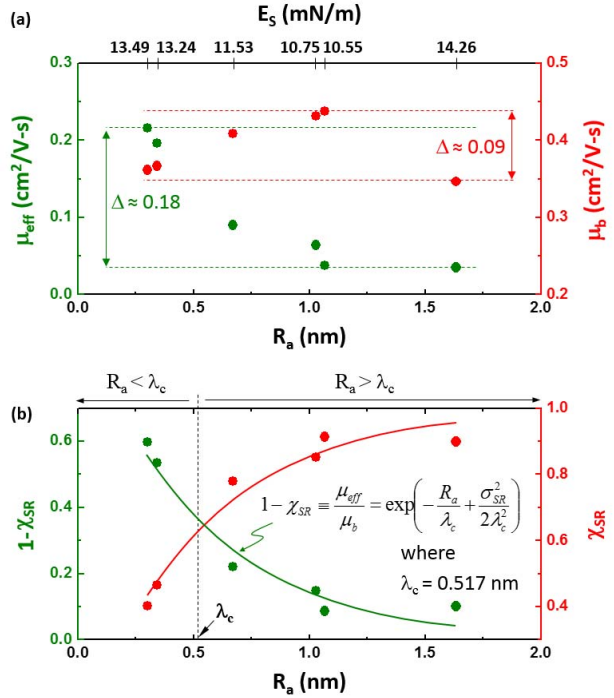


**FIGURE 4.** (a) Effective hole mobility ( $\mu_{\text{eff}}$ ) and reference mobility ( $\mu_b$ ) as a function of the surface roughness ( $R_a$ ). (b)  $1 - \chi_{SR}$  (i.e.,  $\mu_{\text{eff}} / \mu_b$ ) and the degree of surface roughness scattering ( $\chi_{SR}$ ) as a function of  $R_a$ .

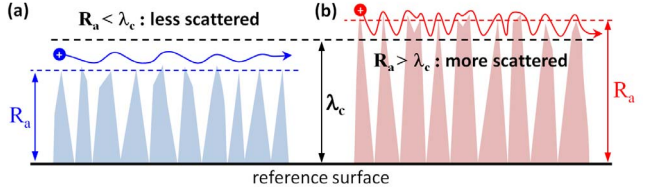


**FIGURE 5.** Conceptual illustrations of the carrier movements when (a) the surface roughness ( $R_a$ ) is smaller than the characteristic scattering length ( $\lambda_c$ ) and (b) when  $R_a$  is larger than  $\lambda_c$ , respectively.

approaches unity when  $R_a > 0.517$  nm, as seen in Fig. 4(b). This suggests that  $\lambda_c$  can be a demarcation for  $R_a$ . These discussions are conceptually illustrated in Fig. 5. Here, we believe that this kind of the demarcation with  $\lambda_c$  provides a quantitative guideline on how much  $R_a$  needs to be reduced for a higher mobility.

### III. CONCLUSION

A quantitative analysis showed that the effective hole mobility in the examined PQT-12 thin film transistor hybridized with the OTS SAM and oxygen plasma treatments is composed of the product of the reference mobility and the surface roughness scattering-related terms. Here, the degree of the surface roughness scattering is inversely proportional to the surface roughness through their exponential relationship derived based on the Gaussian distribution along with the concept of the characteristics scattering length, and the reference mobility follows a power-law as a function of

the surface energy. In particular, the introduced parameter, a characteristics scattering length, can be treated as a demarcation on how much the surface roughness needs to be reduced for a higher mobility. And it was suggested that the surface roughness is required to be scaled to be at least smaller than the characteristics scattering length to reduce the surface roughness scattering, yielding a higher mobility. In the transistor examined here, the characteristics scattering length is found to be 0.517 nm for the OTS SAM PQT-12. Consequently, the analysis presented here gives quantitative and analytical insights into surface properties, which determine the electrical performance and stability of thin film transistors.

## REFERENCES

- [1] J. Y. Oh *et al.*, "Intrinsically stretchable and healable semiconducting polymer for organic transistors," *Nature*, vol. 539, no. 7629, pp. 411–415, Nov. 2016, doi: [10.1038/nature20102](https://doi.org/10.1038/nature20102).
- [2] T. Sekitani, U. Zschieschang, H. Klauk, and T. Someya, "Flexible organic transistors and circuits with extreme bending stability," *Nat. Mater.*, vol. 9, pp. 1015–1022, Nov. 2010, doi: [10.1038/nmat2896](https://doi.org/10.1038/nmat2896).
- [3] Y. D. Park, J. A. Lim, H. S. Lee, and K. Cho, "Interface engineering in organic transistors," *Mater. Today*, vol. 10, no. 3, pp. 46–54, Mar. 2007, doi: [10.1016/S1369-7021\(07\)70019-6](https://doi.org/10.1016/S1369-7021(07)70019-6).
- [4] B. S. Ong, Y. Wu, P. Liu, and S. Gardner, "High-performance semiconducting polythiophenes for organic thin-film transistors," *J. Amer. Chem. Soc.*, vol. 126, no. 11, pp. 3378–3379, Mar. 2004, doi: [10.1021/ja039772w](https://doi.org/10.1021/ja039772w).
- [5] F. M. Li *et al.*, "Polymer thin film transistor without surface pre-treatment on silicon nitride gate dielectric," *Appl. Phys. Lett.*, vol. 93, no. 7, pp. 1–3, Apr. 2008, doi: [10.1063/1.2927485](https://doi.org/10.1063/1.2927485).
- [6] C. Tanase, E. J. Meijer, P. W. M. Blom, and D. M. de Leeuw, "Local charge carrier mobility in disordered organic field-effect transistors," *Org. Electron.*, vol. 4, no. 1, pp. 33–37, 2003.
- [7] C. Jiang, H. Ma, D. G. Hasko, X. Guo, and A. Nathan, "A lewis-acid monopolar gate dielectric for all-inkjet-printed highly bias-stress stable organic transistors," *Adv. Electron. Mater.*, vol. 4, no. 8, pp. 1–7, Jun. 2017, doi: [10.1016/S1566-1199\(03\)00006-5](https://doi.org/10.1016/S1566-1199(03)00006-5).
- [8] L. L. Kosbar, C. D. Dimitrakopoulos, and D. J. Mascaro, "The effect of surface preparation on the structure and electrical transport in an organic semiconductor," in *Proc. Mater. Res. Soc. Symp.*, vol. 665, 2001, Art. no. C10.6.1, doi: [10.1557/PROC-665-C10.6](https://doi.org/10.1557/PROC-665-C10.6).
- [9] M. W. Lee and C. K. Song, "Oxygen plasma effects on performance of pentacene thin film transistor," *Jpn. J. Appl. Phys.*, vol. 42, pp. 4218–4221, Jul. 2003, doi: [10.1143/JJAP.42.4218](https://doi.org/10.1143/JJAP.42.4218).
- [10] E. Carlos *et al.*, "Boosting electrical performance of high-k nanomultilayer dielectrics and electronic devices by combining solution combustion synthesis and UV irradiation," *ACS Appl. Mater. Interfaces*, vol. 9, no. 46, pp. 40428–40437, Nov. 2017, doi: [10.1021/acsm.7b11752](https://doi.org/10.1021/acsm.7b11752).
- [11] E. Fortunato, P. Barquinha, and R. Martins, "Oxide semiconductor thin-film transistors: A review of recent advances," *Adv. Mater.*, vol. 24, no. 22, pp. 2945–2986, May 2012, doi: [10.1002/adma.201103228](https://doi.org/10.1002/adma.201103228).
- [12] F. M. Li, A. Nathan, Y. Wu, and B. S. Ong, "A comparative study of plasma-enhanced chemical vapor gate dielectrics for solution-processed polymer thin-film transistor circuit integration," *J. Appl. Phys.*, vol. 104, pp. 1–12, Oct. 2008, doi: [10.1063/1.3029704](https://doi.org/10.1063/1.3029704).
- [13] F. M. Li, A. Nathan, Y. Wu, and B. S. Ong, "Organic thin-film transistor integration using silicon nitride gate dielectric," *Appl. Phys. Lett.*, vol. 90, pp. 1–3, Feb. 2007, doi: [10.1063/1.2718505](https://doi.org/10.1063/1.2718505).
- [14] T.-M. Pan, C.-H. Chen, J.-H. Liu, J.-L. Her, and K. Koyama, "Electrical and reliability characteristics of high-k  $\text{HfTiO}_3$   $\alpha$ - $\text{InGaZnO}$  thin-film transistors," *IEEE Electron Device Lett.*, vol. 35, no. 1, pp. 66–68, Jan. 2014, doi: [10.1109/LED.2013.2287349](https://doi.org/10.1109/LED.2013.2287349).
- [15] F. Shan *et al.*, "Low-voltage high-stability  $\text{InZnO}$  thin-film transistor using ultra-thin solution-processed  $\text{ZrO}_x$  dielectric," *IEEE/OSA J. Display Tech.*, vol. 11, no. 6, pp. 541–546, Jun. 2015, doi: [10.1109/JDT.2014.2366933](https://doi.org/10.1109/JDT.2014.2366933).
- [16] D. Lu *et al.*, "Surface treatment of indium tin oxide by oxygen-plasma for organic light-emitting diodes," *Mater. Sci. Eng. B*, vol. 97, no. 2, pp. 141–144, Jan. 2003, doi: [10.1016/S0921-5107\(02\)00435-X](https://doi.org/10.1016/S0921-5107(02)00435-X).
- [17] S. M. Rossnagel, W. D. Westwood, and J. J. Cuomo, *Handbook of Plasma Processing Technology: Fundamentals, Etching, Deposition, and Surface Interactions*. New York, NY, USA: Noyes, 1990.
- [18] M. L. Chabiny *et al.*, "Effects of the surface roughness of plastic-compatible inorganic dielectrics on polymeric thin film transistors," *Appl. Phys. Lett.*, vol. 90, no. 23, pp. 1–3, May 2007, doi: [10.1063/1.2746955](https://doi.org/10.1063/1.2746955).
- [19] T. Umeda, D. Kumaki, and S. O. Tokito, "Surface-energy-dependent field-effect mobilities up to  $1 \text{ cm}^2/\text{V s}$  for polymer thin-film transistor," *J. Appl. Phys.*, vol. 105, no. 2, pp. 1–5, Dec. 2009, doi: [10.1063/1.3072669](https://doi.org/10.1063/1.3072669).
- [20] D. K. Owens and R. C. Wendt, "Estimation of the surface free energy of polymers," *J. Appl. Polym. Sci.*, vol. 13, no. 8, pp. 1741–1747, Aug. 1969, doi: [10.1002/app.1969.070130815](https://doi.org/10.1002/app.1969.070130815).



**SUNGSIK LEE** received the Ph.D. degree from the University College London, London, U.K., in 2013. He has been a Professor with Pusan National University, Pusan, South Korea, since 2017. From 2013 to 2017, he was a Research Associate with the University of Cambridge, Cambridge, U.K.. His area of expertise is semiconductor devices and physics for futuristic electronics. He has published over 70 articles and with an *H*-index of 17. He was a recipient of the IEEE EDS Ph.D. student fellowship 2011 and the Best Teaching Prize 2017 from the Korean Society for Engineering Education, South Korea.



**FLORA M. LI** received the Ph.D. degree in electrical engineering from the University of Waterloo, specialized in thin film electronics based on metal oxide semiconductors, organic semiconductors, and nanomaterials. She is currently a Multidisciplinary Researcher and a Program Manager with Apple, passionate about developing new technologies and solutions to make the world a better place. Her specialties lie in research, fabrication process development, material science, engineering, device/material characterization, circuit design and testing, system integration, and project management.



**AROKIA NATHAN** holds the Chair of photonic systems and displays with the Department of Engineering, Cambridge University. He was a Post-Doctoral Fellow with LSI Logic Corporation, USA, and ETH Zurich, Switzerland, for several years. He joined the University of Waterloo, ON, Canada, where he held the DALSA/NSERC Industrial Research Chair in sensor technology and, subsequently, the Canada Research Chair in nano-scale flexible circuits. In 2006, he became the Sumitomo Chair of nanotechnology with the London Centre for Nanotechnology, University College London. He has held Visiting Professor appointments with the Physical Electronics Laboratory, ETH Zurich, and the Engineering Department, Cambridge University, U.K. He has published over 500 papers in the field of sensor technology, CAD, and thin-film transistor electronics, and has co-authored four books. He has over 70 patents filed/awarded and has founded/co-founded four spin-off companies. He was a recipient of the Royal Society Wolfson Research Merit Award from University College London. He serves on technical committees and editorial boards in various capacities. He is a Chartered Engineer, U.K., a fellow of the Institution of Engineering and Technology, U.K., and an IEEE/EDS Distinguished Lecturer.